CAA: Studying the in-medium nuclear effects on the nucleon gluon distribution with vector meson production.

Pierre Chatagnon[1],
Richard Tyson[2]

[1]Irfu/DPhN, CEA, F91191 Gif-sur-Yvette, France
[2]Thomas Jefferson National Accelerator Facility, Newport News, Virginia 23606

September 5, 2025

Abstract

In this CAA, we are proposing to measure the production of vector meson on bound nucleon from nuclear targets. These measurements are expected to be sensitive to the gluon content of the nucleon in nuclear medium. The comparison of these results with existing measurement on free proton and neutron will provide insights on the modification of the gluon content of bound nucleons. The reactions which are planned to be investigated included the photoproduction of both J/ψ and ϕ meson on proton, as well as the hard electroproduction of ϕ on bound proton and neutron. The full datasets from RG-D and RG-E will be used.

Contents

1 Introduction

The impact of the nuclear medium on nucleon structure functions is a well known but as of yet not convincingly understood effect, dubbed EMC after the European Muon Collaboration that first reported this effect. In recent years, measurements of J/ψ photoproduction at JLab [1, 2, 3] have been used to estimate the gluonic mechanical properties of the nucleon, such as mass or pressure distributions of the gluonic content of the nucleon, whilst the production of ϕ has also been predicted to contain information on the gluon and strangeness mechanical properties of the nucleon [4, 5]. A recent measurement in JLab's Hall D has also sought to estimate the J/ψ photoproduction cross section on protons bound in various nuclear targets [6]. This latter measurement was statistically limited but has interesting hints towards the deformation of the gluonic properties of nucleons within nuclear targets, pointing towards a possible gluon EMC effect. In this CAA, we propose to measure the production of J/ψ and ϕ on the bound nucleon of nuclear targets. Especially, we will measure the following reactions:

- $eN \to (e')\gamma N \to (e')J/\psi\ N' \to (e')e^+e^-N'$
- $eN \to (e')\gamma N \to (e')J/\psi\ N' \to (e')\mu^+\mu^-N'$
- $eN \to (e')\gamma N \to (e')\phi\ N' \to (e')e^+e^-N'$
- $eN \to (e')\gamma N \to (e')\phi\ N' \to (e')\mu^+\mu^-N'$
- $eN \to e'\phi\ N' \to e'K^+K^-N'$

where N refers to a nucleon, either the proton or neutron and $eN \to (e')\gamma N \to (e')V$ refers to the photoproduction of a vector meson V on the nucleon, for V either ϕ or J/ψ. These measurements will be done using the RG-D and RG-E datasets, with Deuterium (D2), Carbon (C), Aluminium (Al), Copper (Cu), Tin (Sn) and Lead (Pb) targets. The total and t-differential cross sections will be studied, with the latter allowing to estimate the mechanical properties of the nucleon, providing possible insights into nuclear deformations of the gluonic properties of the nucleon.

2 Physics motivation

It has long been predicted that the J/ψ and ϕ photoproduction cross section can be related to the gluonic content of the nucleon. In Ref. [7] a two gluon production mechanism is used to predict the J/ψ and ϕ near-threshold cross sections, accurately reproducing the existing measurements of the differential cross sections as a function of transfered momentum squared t. In the vector meson dominance model (VMD), a photon beam fluctuates into a vector meson, such as J/ψ or ϕ. The large mass of the vector meson and the requirement for the proton to stay intact despite the large minimum momentum transfer at threshold places kinematic constraints on the quark content of the nucleon, favoring higher twist production mechanisms such as two or three gluon exchanges [8] . This two gluon exchange allows to probe the gluonic content of the nucleon, enabling interesting insights into the nucleon gluonic structure. For example, the mass radius of the nucleon, which can be thought of as the distribution of gluons in the nucleon, has been studied from J/ψ and ϕ photoproduction data [9, 10, 11], with the mass radius of the deuteron being estimated from ϕ photoproduction data [12]. The nucleon mass can also be decomposed into the quark energy contribution, the gluon energy contribution , the quark mass contribution, and the trace anomaly contribution [13]. The magnitude of the contribution of the trace anomaly to the proton mass was estimated from J/ψ photoproduction, allowing to calculate the proton mass from first principles [14, 15]

The 12 Gev upgrade at the JLab has allowed to probe J/ψ near-threshold photoproduction, with measurements released by the GlueX collaboration [1, 2] and the J/ψ-007 collaboration based in Hall C [3], with preliminary measurements on the free proton and bound proton and neutron currently in CLAS collaboration review [16, 17]. Along with providing measurements of the differential cross section as a function of t in the energy region close to the J/ψ production threshold, this has also pushed the theoretical modeling of near-threshold J/ψ photoproduction, in part demonstrating that VMD based models are unsuited to describe the high J/ψ mass [18]. More importantly, the improvement of the

theoretical description of J/ψ near-threshold photoproduction has allowed to relate these measurements to the mechanical structure of the nucleon, which is defined by analogy to General Relativity via the QCD energy-momentum tensor (EMT). The nucleon gravitational form factors (GFFs) $A(t)$, $B(t)$, $D(t)$ and $\bar{C}(t)$ are defined using the matrix elements of the QCD energy-momentum tensor $T^{\alpha\beta}_{q,g}$:

$$\langle p'|T^{\alpha\beta}_{q,g}|p\rangle = \bar{u}(p')\left[A_{q,g}(t)\,\gamma^{(\alpha}P^{\beta)}+B_{q,g}(t)\,\frac{P^{(\alpha}i\sigma^{\beta)\nu}\Delta_\nu}{2M}+D_{q,g}(t)\,\frac{\Delta^\alpha\Delta^\beta-g^{\alpha\beta}\Delta^2}{4M}+\bar{C}_{q,g}(t)\,Mg^{\alpha\beta}\right]u(p), \tag{1}$$

where α, β are indices of the energy-momentum tensor, p and p' are the momenta of the target and recoil nucleon in an electroproduction interaction, $P = \frac{p+p'}{2}$, $\Delta = p' - p$, the Mandelstam variable $t = \Delta^2$, $u(p)$ is the Dirac spinor, and M is the nucleon mass [19]. Note that the energy-momentum tensor can be decomposed into gauge-invariant quark and gluon parts referenced by q, g. The two most prominent models relating vector meson photoproduction to the nucleon GFFs utilise the Generalized Parton Distributions (GPDs) or Holographic QCD frameworks. In the GPD framework, large skewness at threshold allows to relate the scattering amplitude to gluon GPDs. The GFFs are extracted from the Mellin moments of the GPDs [20, 21, 22]. In holographic QCD, a higher dimensional duality relates spin-2 fields, such as a two gluon exchange, to gravity. In this higher dimensional space, J/ψ is produced by the exchange of gravitons (tensor 2^{++} glueballs) and scalar (0^{++}) glueballs, allowing to probe the nucleon GFFs [23, 24].

The J/ψ-007 data has been used to estimate the $A(t)$, and $D(t)$ gluonic GFFs, which in turn allows to extract mass, pressure and shear stress distributions of the gluonic content of the proton, while the upcoming CLAS12 measurements will increase the precision of these extractions. Although these frameworks have focused on J/ψ photoproduction as the larger mass better justifies the use of perturbative QCD approaches, recent work has demonstrated that ϕ photoproduction would also give access to the nucleon GFFs. Interestingly, the predictions show that a higher Q^2 reach would allow to study not only the gluonic but also strangeness properties of the nucleon [4, 5].

Whereas the gluonic properties of the free proton have benefited from several independent measurements of J/ψ photoproduction, the same is not true for the bound nucleon. Preliminary measurements of ϕ photoproduction on the proton in its di-lepton decay channel with CLAS12 offered some glimpses into the gluonic structure of the bound nucleon [25], whilst there also exist further extractions of the gluonic mass radius of bound nucleons from the production of ω and ϕ vector mesons in CLAS, CBELSA/TAPS and LEPS data [11]. Interestingly, these extractions report a larger mass radius for the bound nucleon. One possible interpretation of a larger mass radius of bound nucleons is the *nucleon swelling* picture that explains the nuclear medium modifications of parton distribution functions as a result of differences in the scale of confinement of free and bound nucleons. In this picture, the confinement volume of constituent gluons and quarks increases in the nuclear medium, leading to an increase in the effective nucleon quark and gluon radius [11, 26, 27]. However, all these extractions of the mass radius of the nucleon in deuterium are based on VMD models that were developed for the heavier J/ψ meson, and further shown to be inadequate [18]. Furthermore, more recent modeling of the nucleon GFFs in the GPD based models recommend to measure ϕ electroproduction at Q^2 several times larger than the momentum transfer t [4, 5]. Whilst there exist some previous measurements of ϕ electroproduction on the proton from CLAS, these unfortunately report the differential cross section as a function of t over a large Q^2 range, which prohibits the extraction of the gluon and strange GFFs [28, 4, 5]. No measurements of ϕ electroproduction on the bound proton exist.

The most relevant measurements to study the gluonic properties of bound nucleons in nuclei have been taken at CLAS12 and Hall D. CLAS12 will provide first insights into the mass, pressure and shear stress distributions of the bound proton and neutron in deuterium from J/ψ photoproduction data [17]. However, these measurements do not have the necessary statistical precision to estimate the impact of the nuclear medium on the gluonic properties of the nucleon. Drawing a parallel to the fact that the EMC effect is larger in heavier nuclear targets, a gluon EMC effect could be easier to observe when producing ϕ or J/ψ on the bound nucleon in heavier nuclear targets. Recent results from Hall D published the J/ψ photoproduction cross section on deuterium, helium, and carbon [6]. In

particular, these measurements report the first observation of sub-threshold production of J/ψ where the Fermi momentum of the bound nucleon target conspires with the beam to produce J/ψ at beam energies below its energy threshold. The data suggests an excess of the measured cross section for subthreshold production, which could hint to modified gluon structure for bound protons [6]. Higher precision measurements are necessary to confirm these possible effects and a proposal to extend these measurements to a longer run time on a helium target in Hall D was accepted by the 53rd Jefferson Lab Program Advisory Committee [29].

In this CAA, we propose to use existing CLAS12 data to improve on previous measurements of the nuclear modification of the gluonic properties of the nucleon in several ways. Firstly, we plan to measure J/ψ quasi-real photoproduction on the bound nucleon on a larger range of nuclear targets from deuterium to lead. Possible statistical limitations due to a low cross section for near-threshold J/ψ photoproduction will be mitigated by also measuring ϕ production on the nucleon in these same nuclear targets. Contrary to previous measurements of ϕ production on the nucleon in deuterium that were made at $Q^2 = 0$, our proposed measurements will have a range of Q^2 up to several GeV and allow multidimensional binning in Q^2 and t. Overall, the proposed measurements will greatly impact the current understanding of the gluonic mechanical properties of the nucleon and how these are modified by the nuclear medium.

3 Analysis procedure

In this section, the analysis procedure to select event of interest for the reactions $ep \to (e')\gamma p \to (e')J/\psi\ p' \to (e')e^+e^-p'$ and $ep \to e'\phi\ p' \to e'K^+K^-p'$ is detailed. The datasets on which these measurements will be performed are clearly stated and a list of observables and the steps to compute them are given for both analysis.

3.1 Dataset

The measurements proposed in this CAA will be performed on nuclear dataset taken during the RG-D and RG-E run periods. We plan to use both datasets as each is using a different torus field polarity. Each target dataset of each run group will be analyzed separately. Table 1 summarizes the different datasets and the measurements that will be performed. Note that ϕ photoproduction is only measurable in the inbending torus polarity, limiting its measurements to RG-E dataset. The following pilot studies have been done on roughly 10% of the total RG-D dataset, available as of the 1st of September 2025.

Run group	Target	$J/\psi \to e^+e^-$	$J/\psi \to \mu^+\mu^-$	$\phi \to e^+e^-$	$\phi \to \mu^+\mu^-$	$\phi \to K^+K^-$
RG-D	LD2	✓	✓			✓
	C					
	Cu					
	Sn					
RG-E	LD2	✓	✓	✓	✓	✓
	Sn					
	Al					
	Pb					

Table 1: Summary of the proposed vector meson measurements for each dataset and each target.

3.2 $J/\psi \to e^+e^-$ preliminary analysis on RG-D data

3.2.1 Particle identification

The final state of interest for the reaction of photoproduction of J/ψ is composed of a proton, an electron and a positron. All three final state particles are selected using the standard CLAS12 event builder [30]. No additional cut is applied to the proton in this pilot analysis. The complete analysis will include additional cuts on the proton χ^2_{PID}.

Additional cuts are applied on both of the final state electron and the positron. Especially, we use the BDT-based lepton PID developed for the TCS and J/ψ analysis of RG-A [31, 16] and fully documented in [32]. The effect of using such an algorithm on positron from the CuSn dataset of RG-D is illustrated in Figure 1. This pilot study demonstrates that using an additional level of PID for lepton is necessary and using the algorithm developed for RG-A already provides good performances. The complete analysis will involve developing a version this BDT-based algorithm for RG-D and RG-E datasets.

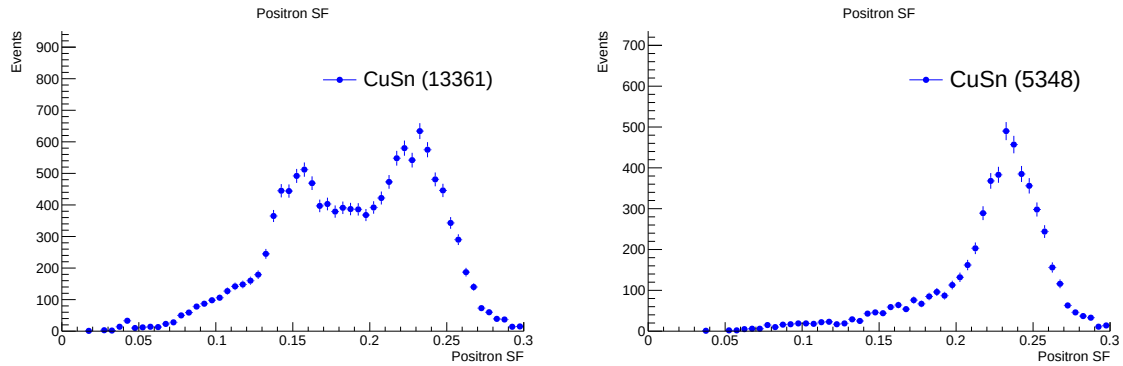

Figure 1: Left: Sampling Fraction for all positrons with momentum larger than 1.5 GeV in the CuSn dataset. Right: Sampling fraction for positrons with momentum larger than 1.5 GeV and Lepton-ID BDT score larger than 0.13, removing most of the pion contamination.

3.2.2 RG-D target selection and vertex cut

Because of the RG-D target geometry, additional cuts on the lepton vertices are applied. Figure 2 shows the vertex distributions of the electron vertex for events with the selected final state of interest. In order to keep events produced by the nuclear foils, a cut on both the electron and positron vertex is applied (-10 cm $< v_z < 0$ cm). Note that due to the lack of statistics available for this pilot study, in the case of the CuSn target, no cut is applied to separate the copper to the tin target, and all events from either of target is considered in the following figures. For the complete analysis, each target will be analysed separately.

3.2.3 Event selection and Signal extraction

Events with exactly one proton, one electron, and one positron (including additional PID and vertex cut detailed before) are selected for this preliminary analysis. Lepton momenta are requiered to be above 1.5 GeV. The virtuality of the initial photon $\tilde{Q}^2$ and the missing mass of the undetected scattered electron M_X^2 can be reconstructed as:

$$\tilde{Q}^2 = 2 \cdot E_{beam} \cdot E_X (1 - \cos\theta_X), \tag{2}$$

and

$$M_X^2 = (p^\mu_{beam} - (p^\mu_p + p^\mu_{e^+} + p^\mu_{e^-} - p^\mu_{target}))^2, \tag{3}$$

where the missing particle kinematics θ_X and E_X are reconstructed from momentum-energy conservation. All these computations assume that the target proton is at rest in the nucleus. This hypothesis is necessary at this stage of the analysis as the scattered electron is not reconstructed.

Figure 3 shows the $\tilde{Q}^2$ versus M_X^2 plane for each target of the RG-D dataset. An enhancement can be seen in the region where $\tilde{Q}^2$ and M_X^2 are small. With increasing A, the resolution on both $\tilde{Q}^2$ and M_X^2 increases. This is due to the Fermi motion of the initial proton in the target nucleus. This effect will be studied using Monte-Carlo simulations in the complete analysis.

To select the events of interest, a cut on both $\tilde{Q}^2$ and M_X^2 is applied:

$$0 \text{ GeV}^2 < \tilde{Q}^2 < 1 \text{ GeV}^2, \tag{4}$$

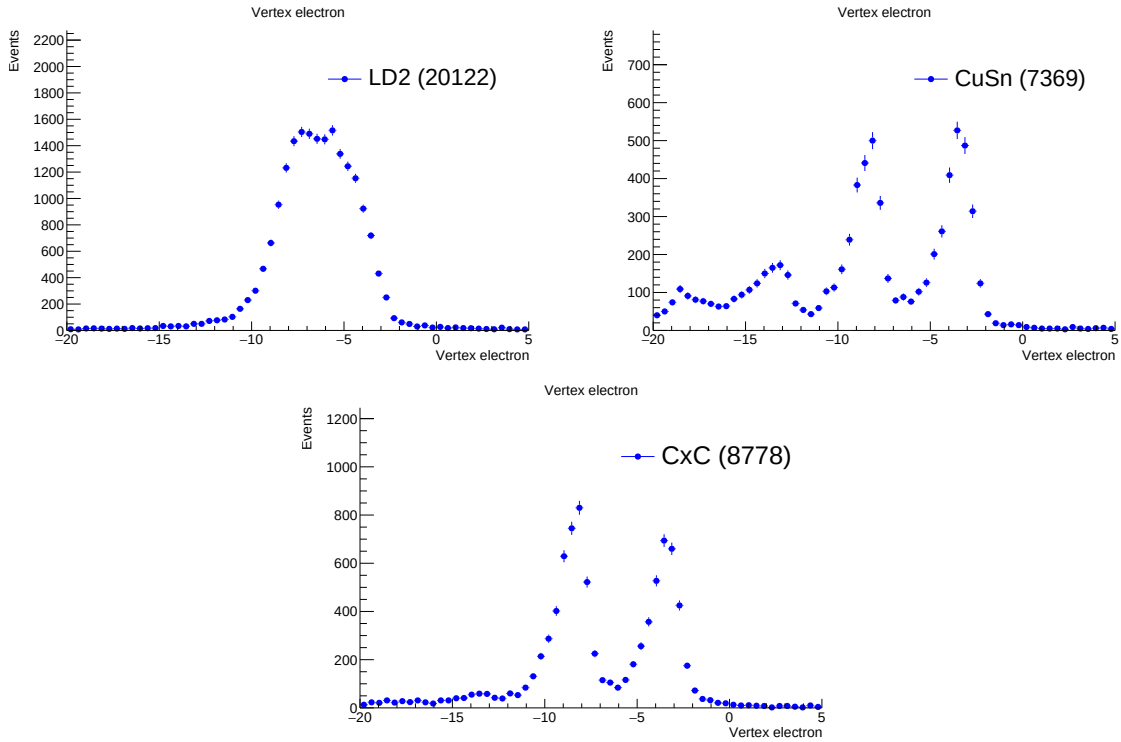

Figure 2: Reconstructed electron vertex for the LD2 target (top left), the CuSn target (top right), and the CxC target (bottom).

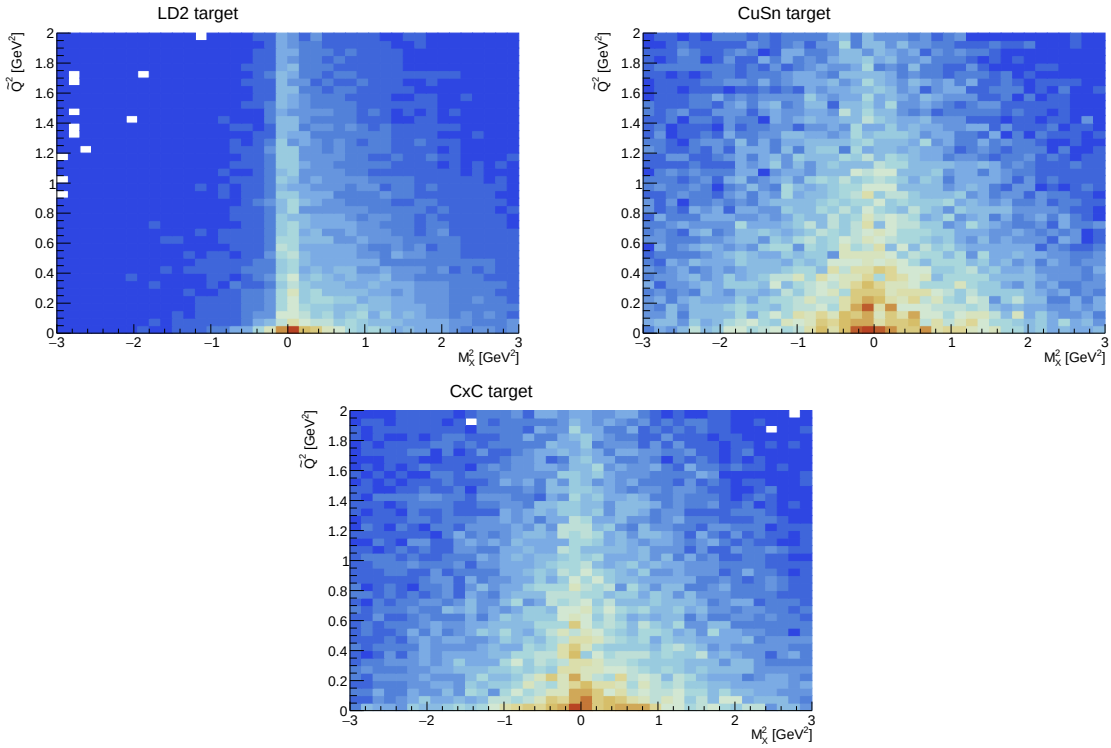

Figure 3: Reconstructed inital photon virtuality $\tilde{Q}^2$ as a function of the missing mass of the scattered electron M_X^2 for the LD2 target (top left), the CuSn target (top right), and the CxC target (bottom).

and

$$|M_X^2| < 3 \text{ GeV}^2. \tag{5}$$

Figure 4 shows the invariant mass of the lepton pair for each target configuration of RG-D, once the exclusivity cuts are applied. The J/ψ peak is fitted with a Gaussian and a second-order polynomial background, and the corresponding number of J/ψ is given for each target. Considering that this preliminary analysis is done with roughly 10% of the total RG-D dataset, we expect 200 events on the LD2 target, 100 events on the CuSn target and 70 on the carbon target. We expect to at least double the statistics by adding the RG-E dataset, as the inbending torus configuration has shown to provide larger acceptance for this reaction (see [16]).

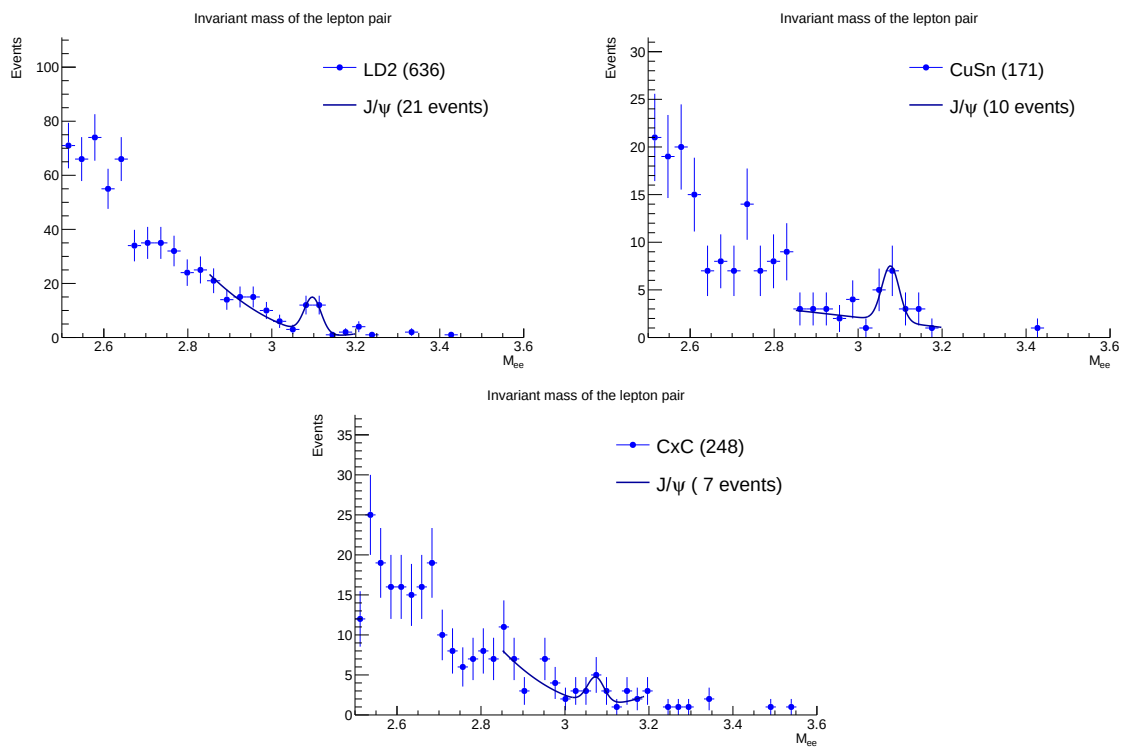

Figure 4: Fitted invariant mass of the lepton pair for the LD2 target (top left), the CuSn target (top right), and the CxC target (bottom).

3.2.4 Observables

For J/ψ photoproduction, we aim at measuring the dependence of the cross section with t and the total cross section as a function of the initial photon energy. The following steps will need to be completed:

- Development of a realistic event generator including radiative corrections,
- Efficiency correction,
- Cross section normalization,
- Understanding of the Fermi motion effect.

To complete these steps, we will use the experience acquired during both the analysis of the same reaction on proton and neutron targets, in RG-A [16] and RG-B [17]. Especially, robust ways of estimating the efficiency of CLAS12 have been developed, either estimating single particle efficiencies or using a complete description of all signal and background in region where it is fully understood (i.e., in the continuum region to the left of the J/ψ peak). We plan to base this analysis on similar methods.

3.2.5 Additional measurements in the dilepton channel

We also propose to measure the same reaction using the di-muon final state. A BDT-based muon identification algorithm has been developed with success for RG-A and RG-B [25]. We expect that using similar approach in RG-D and RG-E will yield good results, as the overall algorithm architecture and input variables are similar to the lepton-PID algorithm presented in section 3.2.1. Using the di-muon final state will double the expected statistics for all targets.

3.3 $\phi \to K^+K^-$ preliminary analysis on RG-D data

The same datasets are used for the preliminary ϕ signal extraction as those used for J/ψ, namely roughly 15 RG-D outbending runs on each of the LD2, CxC and CuSn targets, available on the 1st of September 2025. The preliminary analysis presented here demonstrates the feasibility of the final analysis.

3.3.1 Particle identification

We aim to study the ϕ production in the kaon pair final state (ie $ep \to e'\phi p \to e'K^+K^-p$ where all final state particles are detected). The electron is detected in the Forward Detector of CLAS12, with the kaon pair and proton detected in both the central and forward detectors to maximize statistics. In this pilot analysis no distinction is done for CD and FD particles, but the complete analyses will separate the measurements based on the detector in which the final state particles are detected. The electron and proton are identified using the standard CLAS12 Event Builder PID [30]. The kaons with momenta lower than 3.5 GeV are identified with the event builder PID, whilst those with momenta above 3.5 GeV are only identified by charge. To ensure that final state particles come from the same beam bucket, the absolute value of the difference in vertex time between each particle and the electron is restricted to less than 4ns. Figure 5 shows the velocity versus momentum distributions for each of the kaons and the proton, demonstrating good particle identification.

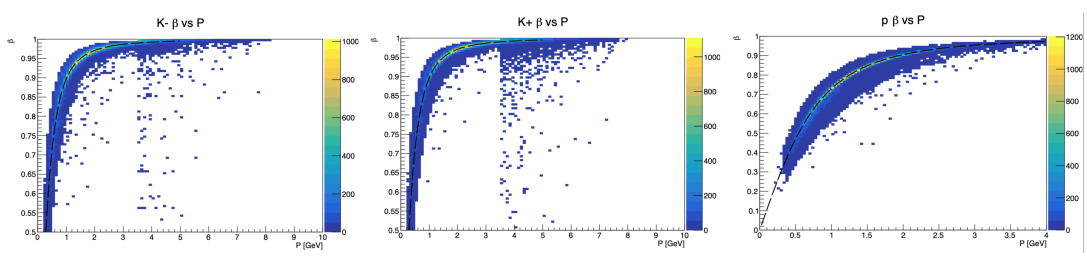

Figure 5: The β versus momentum distribution for negatively charged kaons (left), positively charged kaons (middle) and protons (right). These plots were produced using the data taken with the RG-D LD2 target.

3.3.2 Event selection

In order to select $ep \to e'K^+K^-p$ events, the absolute value of the missing mass squared of $ep \to e'\phi p \to e'K^+K^-p$ is restricted to less than 0.1 GeV^2. The missing mass of $ep \to e'\phi p \to e'K^+K^-(p)$ where the proton is not used in the calculation is restricted to between 0.6 and 1.2 GeV. Note that the cut is preferred when the proton is not used in the calculation rather than kaons as the Fermi motion of the bound proton within the nuclear target would smear the calculation of the missing kaon mass. Figure 6 shows the missing mass and momentum of the reaction $ed \to e'K^+K^-p(n_s)$ on LD2 target, showing a peak close to the neutron mass and an expected Fermi momentum distribution for the missing spectator neutron produced in the breakup of the deuteron target, thus validating the event selection procedure.

Figure 7 shows the Mandelstam -t (left) and Q^2 (right) distributions of $ep \to e'\phi p \to e'K^+K^-p$ taken on the LD2 target. Figure 8 shows the K^+K^- invariant mass when produced on an LD2 target, a CxC target and a CuSn target. For the LD2 and CxC targets, the electron z vertex is restricted to

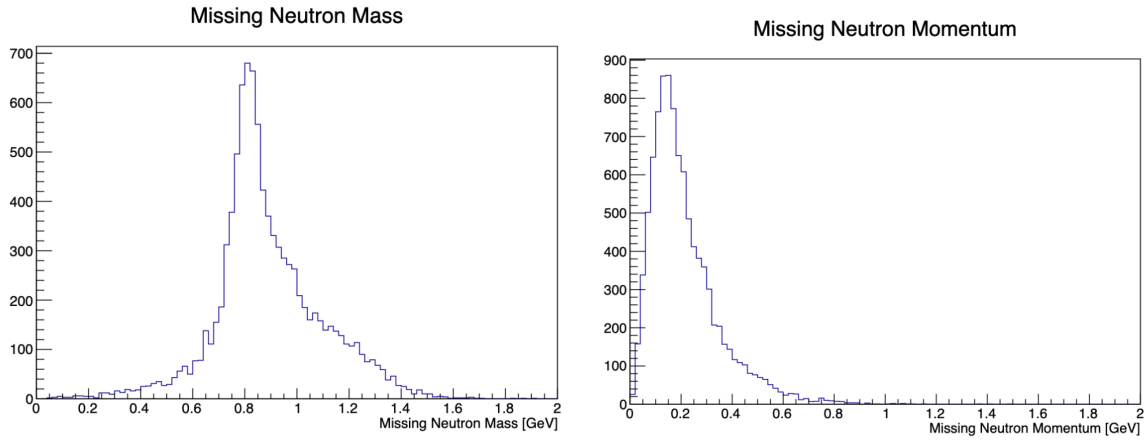

Figure 6: The missing mass (left) and momentum (right) of the $ed \to e'K^+K^-p(n_s)$ where n_s refers to the spectator neutron. These plots were produced using the data taken with the RG-D LD2 target.

-12 to 0 cm, covering the full range of the targets. For the CuSn target, the electron z vertex range is split between -12 to -6 cm for the Cu target and -6 to 0 cm for the Sn target. For all targets, a clear ϕ signal is visible in the K^+K^- invariant mass distributions, ensuring that the full RG-D statistics will allow for a successful and impactful measurement of the ϕ electroproduction on the bound nucleon in nuclear targets. The extension to the RG-E dataset will allow to investigate the cross sections over a different range of targets and in the inbending polarity, providing an independent measurement of ϕ production on the bound nucleon in nuclear targets.

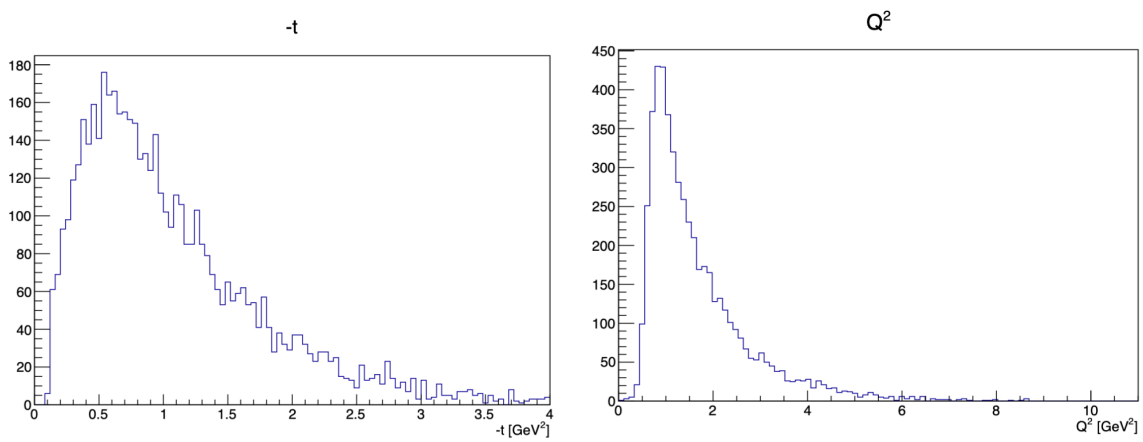

Figure 7: The Mandelstam -t (left) and Q^2 (right) distributions of $ep \to e'\phi p \to e'K^+K^-p$ taken on the LD2 target.

3.3.3 Observables

For this reaction, we are aiming at measuring the dependence of the cross section with t and the virtuality of the incoming photon Q^2. This measurement will require a good understanding of the acceptance and efficiency of CLAS12. In order to finalise the analysis, the following steps will need to be completed:

- Development of a realistic event generator including radiative corrections,
- Efficiency correction,
- Cross section normalisation,

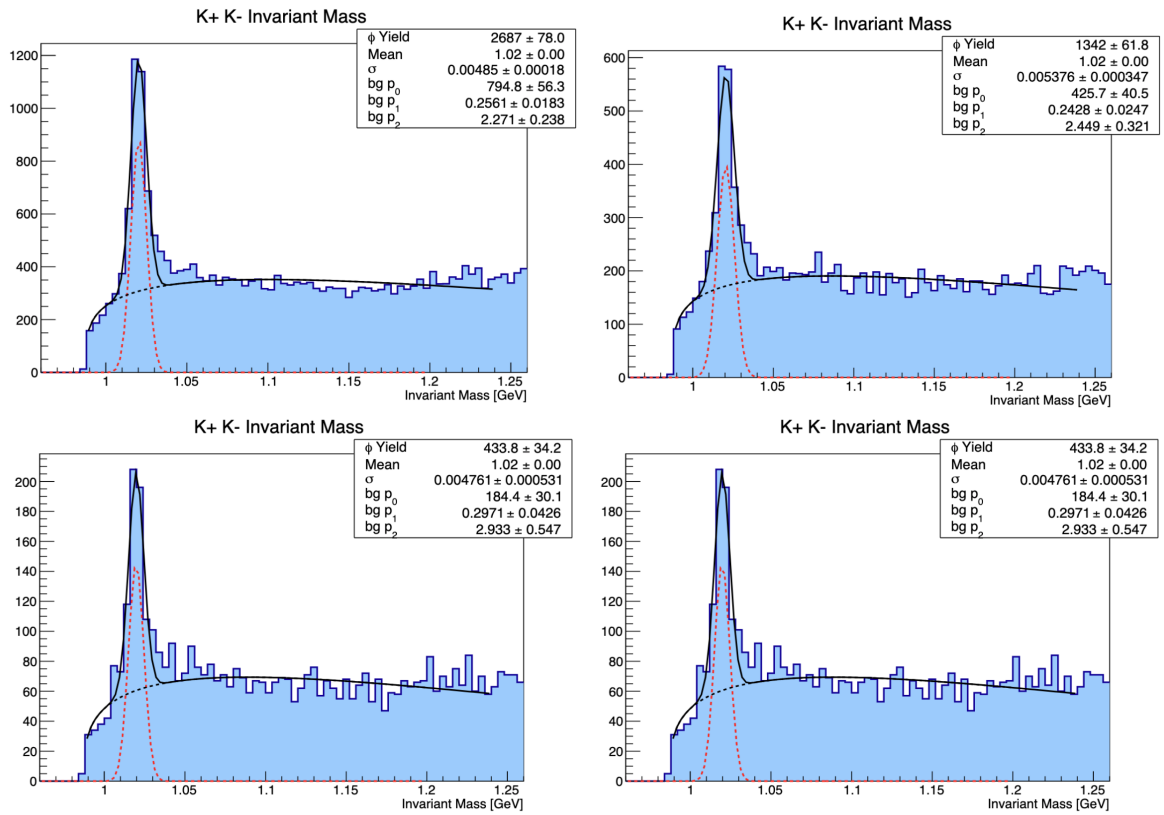

Figure 8: The K^+K^- invariant mass when produced on an LD2 target (top left), a CxC target (top right), a Cu target (bottom left) and a Sn target (bottom right). **N.B.** The uncertainty on the mean is smaller than the precision allowed and so is reported as 0.

- Multi-dimensional binning in Q^2 and t,
- Cross section calculation.

All of these steps will be informed by recent cross section measurements at CLAS12. The main complication will be due to the normalisation of the cross section. As the current version of the GEMC simulation is not fully accurate in reproducing detection efficiencies and resolutions, a correction to the efficiency correction is required to normalise the cross section. The comparison of the cross section measurement between two different datasets, RG-D and RG-E, should give a first estimate of effects that are not well reproduced in GEMC due to the specificities of the targets. Ongoing analyses on a hydrogen target in RG-A will also have to establish a normalisation procedure, and so good synergy between the proposed analysis and other ongoing analyses should allow to establish a detailed normalisation strategy. In the case where this is not feasible, this analysis will look at the ratio of the cross section on a LD2 target to other targets in other to estimate the impact of the nuclear medium on the ϕ production cross section.

4 Summary

The study of J/ψ and ϕ photoproduction on the bound nucleon within nuclear targets has the potential to estimate the impact of the nuclear medium on the gluonic content of the nucleon, providing hints towards a gluonic EMC effect. In this CAA we have demonstrated the feasibility of such an analysis with RG-D data, and expect similar procedures to yield equivalent results on RG-E data. The successful completion of the proposed measurements will greatly improve the current global understanding of the gluonic properties of nucleons within nuclei.

References

[1] A. (et. al.) Ali. First measurement of near-threshold j/ψ exclusive photoproduction off the proton. *Phys. Rev. Lett.*, 123:072001, Aug 2019.

[2] S. (et. al.) Adhikari. Measurement of the j/ψ photoproduction cross section over the full near-threshold kinematic region. *Phys. Rev. C*, 108:025201, Aug 2023.

[3] B. (et. al.) Duran. Determining the gluonic gravitational form factors of the proton. *Nature*, 615(7954):813–816, 2023.

[4] Yoshitaka Hatta and Mark Strikman. ϕ-meson lepto-production near threshold and the strangeness d-term. *Physics Letters B*, 817:136295, 2021.

[5] Yoshitaka Hatta, Henry T. Klest, Kornelija Passek-K., and Jakob Schoenleber. Deeply virtual ϕ-meson production near threshold, 2025.

[6] J.R. (et. al.) Pybus. First measurement of near-threshold and subthreshold j/ψ photoproduction off nuclei. *Phys. Rev. Lett.*, 134(201903), 2025.

[7] L. Frankfurt and M. Strikman. Two-gluon form factor of the nucleon and j/ψ photoproduction. *Phys. Rev. D*, 66:031502, Aug 2002.

[8] S.J. Brodsky, E. Chudakov, P. Hoyer, and J.M. Laget. Photoproduction of charm near threshold. *Physics Letters B*, 498(1):23–28, 2001.

[9] Dmitri E. Kharzeev. Mass radius of the proton. *Phys. Rev. D*, 104:054015, Sep 2021.

[10] Rong Wang, Wei Kou, Ya-Ping Xie, and Xurong Chen. Extraction of the proton mass radius from the vector meson photoproductions near thresholds. *Phys. Rev. D*, 103:L091501, May 2021.

[11] Chengdong Han, Gang Xie, Wei Kou, Rong Wang, and Xurong Chen. The neutron and proton mass radii from the vector meson photoproduction data on the deuterium target. *The European Physical Journal A*, 58(6):105, 2022.

[12] Rong Wang, Wei Kou, Chengdong Han, Jarah Evslin, and Xurong Chen. Proton and deuteron mass radii from near-threshold ϕ-meson photoproduction. *Phys. Rev. D*, 104:074033, Oct 2021.

[13] Xiangdong Ji. Qcd analysis of the mass structure of the nucleon. *Phys. Rev. Lett.*, 74:1071–1074, Feb 1995.

[14] Rong Wang, Xurong Chen, and Jarah Evslin. The origin of proton mass from j/ψ photo-production data. *The European Physical Journal C*, 80(6):507, 2020.

[15] Wei Kou, Rong Wang, and Xurong Chen. Extraction of proton trace anomaly energy from near-threshold ϕ and j/ψ photo-productions. *The European Physical Journal A*, 58(8):155, 2022.

[16] P.Chatagnon et al. Analysis note: Measurement of the cross-section of the photoproduction of the jpsi meson near the production threshold with the clas12 detector. (https://www.jlab.org/Hall-B/shifts/admin/paper_reviews/2025/JPsi_photoproduction_cross_section_in_Hall_B_14.pdf-6791023-2025-07-18-v5.pdf).

[17] R. Tyson et al. Analysis note: Measurement of near-threshold jpsi quasi-real photoproduction on the proton and neutron at clas12. (https://www.jlab.org/Hall-B/shifts/admin/paper_reviews/2025/RGB_Jpsi_Analysis_Note.pdf-1873625-2025-06-17-v1.pdf).

[18] D. Winney, C. Fernández-Ramírez, A. Pilloni, A. N. Hiller Blin, M. Albaladejo, Ł. Bibrzycki, N. Hammoud, J. Liao, V. Mathieu, G. Montaña, R. J. Perry, V. Shastry, W. A. Smith, and A. P. Szczepaniak. Dynamics in near-threshold j/ψ photoproduction. *Phys. Rev. D*, 108:054018, Sep 2023.

[19] V. D. Burkert, L. Elouadrhiri, F. X. Girod, C. Lorcé, P. Schweitzer, and P. E. Shanahan. Colloquium: Gravitational form factors of the proton. *Rev. Mod. Phys.*, 95:041002, Dec 2023.

[20] Yuxun Guo, Xiangdong Ji, and Yizhuang Liu. Qcd analysis of near-threshold photon-proton production of heavy quarkonium. *Phys. Rev. D*, 103:096010, May 2021.

[21] Yuxun Guo, Xiangdong Ji, Yizhuang Liu, and Jinghong Yang. Updated analysis of near-threshold heavy quarkonium production for probe of proton's gluonic gravitational form factors. *Phys. Rev. D*, 108:034003, Aug 2023.

[22] Yuxun Guo, Xiangdong Ji, and Feng Yuan. Proton's gluon gpds at large skewness and gravitational form factors from near threshold heavy quarkonium photoproduction. *Phys. Rev. D*, 109:014014, Jan 2024.

[23] Yoshitaka Hatta and Di-Lun Yang. Holographic j/ψ production near threshold and the proton mass problem. *Phys. Rev. D*, 98:074003, Oct 2018.

[24] Kiminad A. Mamo and Ismail Zahed. j/ψ near threshold in holographic qcd: a and d gravitational form factors. *Phys. Rev. D*, 106:086004, Oct 2022.

[25] R. Tyson. *J/ψ Near-Threshold Photoproduction off the Proton and Neutron with CLAS12*. PhD thesis, University of Glasgow, 2023.

[26] F.E. Close, R.G. Roberts, and G.G. Ross. The effect of confinement size on nuclear structure functions. *Physics Letters B*, 129(5):346–350, 1983.

[27] Rong Wang, Raphaël Dupré, Yin Huang, Baiyang Zhang, and Silvia Niccolai. Flavor-dependent emc effect from a nucleon swelling model. *Phys. Rev. C*, 99:035205, Mar 2019.

[28] J. P. (et. al.) Santoro. Electroproduction of $\phi(1020)$ mesons at $1.4 < q^2 < 3.8$ gev^2 measured with the clas spectrometer. *Phys. Rev. C*, 78:025210, Aug 2008.

[29] Jefferson Lab Program Advisory Committee (PAC 53). Pac 53 report: 53rd program advisory committee meeting, july 21–25, 2025, July 2025.

[30] V. Ziegler (et. al.). The clas12 software framework and event reconstruction. *Nuclear Instruments and Methods in Physics Research Section A: Accelerators, Spectrometers, Detectors and Associated Equipment*, 959:163472, 2020.

[31] P.Chatagnon et al. Timelike compton scattering analysis note. (https://www.jlab.org/Hall-B/shifts/admin/paper_reviews/2021/AnalysisNote-1461061-2021-05-31-v9.pdf).

[32] M. Tenorio-Pita. Clas12 note 2024-005: Enhancing lepton identification in clas12 using machine learning techniques. (https://misportal.jlab.org/mis/physics/clas12/viewFile.cfm/2024-005.pdf?documentId=172).